X-620-70-242

PREPRINT

NASA TM X-63954

THE DAYSIDE IONOSPHERE OF VENUS

J. R. HERMAN
R. E. HARTLE
S. J. BAUER

JUNE 1970

GODDARD SPACE FLIGHT CENTER
GREENBELT, MARYLAND

THE DAYSIDE IONOSPHERE OF VENUS

by

J.R. Herman, R.E. Hartle and S.J. Bauer
Laboratory for Planetary Atmospheres
Goddard Space Flight Center
Greenbelt, Maryland

ABSTRACT

Theoretical modeling of the daytime Venus ionosphere is used to augment the measurements of Mariner V made during its 1967 flyby of Venus. The equations of heat transport for the electron, ion, and neutral gases are simultaneously solved along with the associated momentum and chemical equations for the ion and neutral gas densities. When solutions are constrained by the observations from Mariner V, the resulting temperature and density profiles can be used tc estimate the possible magnetic field strength within the Venus ionosphere and concentration of neutral helium at 100 km altitude. Several alternate models are presented to account for the effects of eddy diffusion in the neutral atmosphere and solar wind heating. In all these models the resulting solutions lead to an approximately horizontal magnetic field in the topside ionosphere of strength 10 - 20γ and a neutral helium density of order 10^{8} cm^{-3} at 100 km altitude.

INTRODUCTION

During the 1967 flyby mission, Mariner V obtained a single cross sectional profile of the day and nighttime Venus ionosphere (Fjeldbo and Eshleman, 1969; Mariner Stanford Group, 1967). This data combined with in situ measurements of the nightside by Venera IV can be used to construct additional features of the Venus ionosphere from theoretical models. The main features observed during the Mariner V encounter are summarized in Figure 1. At the time of observation the solar wind speed was about 590 km/sec with a density of 3 protons cm^{-3} and a kinetic proton temperature of 3×10^{5} °K. The solar wind carried a small magnetic field of strength about 10γ oriented at 26° to the flow streamlines at the orbit of Venus (based on a spiral field model). Upon encountering the highly conducting Venus ionosphere currents are induced to flow so that a magnetic field appears across the front side of the planet. This magnetic field deflects the incoming solar wind particles and guides them around to the back forming a tail-like structure extending many Venus radii (Dessler, 1968; Johnson, 1968). The Mariner V occultation data clearly shows these features in that a sharp cutoff in the electron density (ionopause) occurred at about 500 km on the dayside and 3500 km on the nightside. As shown in the figure, the location of these points was approximately 45° below the subsolar wind point and 135° above, respectively. Waves propagating upstream from the ionopause region give rise to a bow shock as observed in both the density and magnetic field data at about 50,000 km from Venus along the Mariner V entry trajectory.

A model of the solar wind interaction with Venus and its consequences for the ionosphere has been recently discussed (Bauer, et. al., 1970). In this model the streaming energy of the solar wind is converted to magnetic and thermal energy in the region inside the bow shock. The magnetic field strength is expected to rise from about 10γ in the solar wind to about 40γ in the vicinity of the ionopause. Between the bow shock and the ionopause the proton temperature increases to nearly 4×10^6 °K. Within the ionosphere the inward solar wind pressure must be balanced by the sum of the ionospheric charged particle pressure and possible magnetic field pressure. In the ideal case of an infinitely conducting ionosphere, the induced currents corresponding to the solar wind flow lie entirely in the ionopause surface and in the region above. The resulting magnetic field is excluded from the ionosphere. Even with a realistic finite conductivity the magnetic diffusion time t_d is so much greater than the reversal time for the interplanetary magnetic field, that magnetic diffusion into a quiet ionosphere should be negligible. Since t_d is also much larger than a Venus day, the rotation effects and field reversal would have to be considered simultaneously to properly assess the degree of magnetic field penetration. However, if a magnetic field is present within the ionosphere, then it may arise from a weak planetary magnetic moment, from currents generated by large scale inhomogenities, or from enhanced magnetic diffusion. If the effective distance over which the magnetic field can be considered homogeneous is reduced from the order of a planetary radius to a much smaller value (thereby

reducing t_d), magnetic diffusion would become important. This may be possible if the likely turbulence in the topside ionosphere produces a wave structure with small characteristic lengths. The need for some source of magnetic field within the topside ionosphere is borne out by the model calculation presented in the following sections.

BASIS OF THE THEORETICAL MODELS

From the preceeding discussion it is clear that the sun, in addition to the usual EUV radiation effects, strongly influences the Venus ionosphere. In order to assess the effects of solar control on the Venus ionosphere it was necessary to solve the heat transport equations for the electron, ion, and neutral gases simultaneously with the momentum and chemical equations for their temperatures and densities. The equations and parameters used for this study are fully listed in the Appendix, and a detailed discussion of a similar set of equations as applied to the earth's ionosphere has been given previously (Herman and Chandra, 1969).

In addition to the pressure balance boundary condition needed at the ionopause, the values of the neutral densities at the lower boundary, 100 km, are among the most important parameters needed to characterize the ionosphere. In this connection we find that a CO_2 density of 5×10^{13} cm^{-3} with a small amount of N_2(<0.1%) in photochemical equilibrium with their ions reproduces the lower daytime ionosphere quite well. Varying the CO_2 density produces pronounced shifts in the altitude of the electron density maximum as shown in Table 1. That is, we find the calculated electron density maximum occurs at altitudes ranging from 120 km to 145 km as the CO_2 density is varied from 1×10^{12} cm^{-3}. The shift is in direct response to changes in altitude of the maximum solar EUV absorption. Since the topside thermal structure is relatively insensitive to the CO_2 concentration in the range indicated in Table 1, the observed electron density peak of 5.3×10^{5} cm^{-3} at 140 km can be used as an indirect boundary condition that

fixes the density of CO_2 at 100 km at 5×10^{13} cm^{-3}

The concentrations of hydrogen and deuterium at the 100 km base are determined by solving for all the temperature and density profiles simultaneously, and varying the base values of hydrogen and deuterium until the resulting densities are consistent with those inferred from Lyman α measurements at great distances from the planet (Barth, et. al., 1968; Kurt, et . al, 1969). As is described elsewhere (McElroy and Hunten, 1969), one can obtain in this manner hydrogen and deuterium densities of 5×10^{6} and 2×10^{6} cm^{-3} at 100 km, respectively. Molecular hydrogen, while present in the lower ionosphere, is not thought to be an important constituent for the altitude range of interest because of its rapid photodissociation (Dalgarno and Allison, 1969). There is no experimental evidence concerning the quantity of helium in the atmosphere, although an estimate has been made based on an earthlike model of its radiogenic origin (Knudsen and Anderson, 1969). Acccrdingly, we have treated the neutral helium density at 100 km as a parameter of the problem, and have investigated its effect on the charged particle density and temperature distributions.

The boundary conditions for the heat transport equations are specified in terms of temperature gradients for each constituent at the upper boundary (500 km at the dayside Mariner V occultation point) and a common fixed temperature at the lower boundary (100 km). The use of a non-zero temperature gradient at the upper boundary implies a knowledge of the thermal structure above the boundary altitude. Based on a hydromagnetic analysis of the solar wind interaction with the Venus ionosphere

(Spreiter, 1970), the maximum amount of thermal energy available for conduction into the ionosphere is less than 10% of the energy deposited by energetic photo-electrons in the topside. At most this represents a small correction towards higher temperatures and pressures. Accordingly, we have used a zero temperature gradient at the upper boundary, z_u, and have introduced a distributed source of thermal energy in the topside to simulate possible solar wind heating, $Q_{sw} = (\alpha V/\lambda)P_{sw}\exp((z - z_u)/\lambda)$. That is, a fraction α of the solar wind energy flux VP_{sw} is deposited at each altitude z with an e - folding distance λ. We have also included the small amount of heating from the direct coulomb interaction between ambient charged particles and solar wind protons that are able to penetrate the ionopause region (see Q_{ep}, Q_{4p}, Q_{5p} in the Appendix). Even with the maximum possible penetration of solar wind protons, the resulting ionospheric heating is only a 1% perturbation.

Helium ions in the topside ionosphere are produced mainly by photoionization and lost by charge exchange with CO_2, H, D, and electron recombination. For rates appropriate to Venus, the daytime electron density, as measured by Mariner V can be supplied in about 1000 seconds, and so maintained throughout the Venus day of about 10^7 seconds unless the upward velocity of He^+ exceeds 0.5 km/sec. A similar calculation for H^+ including both photoionization and charge exchange yields a filling time of 10^5 seconds and an upper limit on the upward velocity of 0.01 km/sec. Since the Venus day is much longer than both filling times, H^+, D^+, and He^+ are possible constituents of the topside ionosphere with He^+, possibly the dominant ion. This conclusion depends upon the amount of

neutral hydrogen and deuterium present in the topside. That is, H densities in excess of 10^5 cm^{-3} could lead to H^+ as the dominant ion via charge exchange with He^+ and photoionization. The only requirements placed on the model by the data are that the ion scale height be quite large (> 100 km) and that the electron density near the ionopause be 1.2×10^4 cm^{-3}. This can be met by any combination of H^+, D^+, and He^+, the sum of whose densities must be 1.2×10^4 cm^{-3}.

An upward velocity of 0.5 km/sec supplies only 1% of the necessary upward pressure needed to support the topside ionosphere against the solar wind. Equivalently, a supersonic velocity of about 10 km/sec is needed if the pressure balance is shared equally between kinetic and streaming pressure. Such supersonic velocities are not likely to be obtained in a system with horizontal magnetic field lines at the ionopause preventing radial outflow from the planet. When the effects of even moderate upward flow are incorporated into our models, any horizontal components of the magnetic field are carried with the flow and compressed into the topside region just below the ionopause (Banks and Axford, 1970). In this case we find that the electron and ion thermal conduction increases in the field free region thereby causing the temperatures and internal kinetic pressure to fall to somewhat less than half that needed for pressure balance with the solar wind, Figure 2. The pressure deficit can be made up by adjusting the parameters αV and λ in Q_{sw} to supply sufficient additional heating. These effects are discussed later. If the upward flow is limited by the need to maintain the observed electron density in the topside ionosphere, the radial density distribution of light ions is

approximately given by a simple force balance with $V_i \simeq 0$ (see Appendix). The solutions we obtain in this manner yield a large electric field in the region where the ionosphere changes from CO_2^+ to one of the light ions, Figure 3 ($E \simeq 20\ m_{H^+} e/g$, where g = the acceleration of gravity). Newly created hydrogen ions would be accelerated by this large field creating an upward flux that might contribute significantly to the pressure balance. The result is that hydrogen ions would steam upwards at 6 to 8 km/sec with a flux of about 10^7 cm^{-2} sec^{-1}. The flux is estimated by setting $div(nV) \sim PL$ where the production rate $P \lesssim 1$ cm^{-3} sec^{-3} sec^{-1} and $L \sim 100$ km). The resulting upward pressure from such a flux at the ionopause region is a maximum of 1×10^{-11} dynes cm^{-2} as compared to the solar wind pressure at the occultation point of 8×10^{-9} dynes cm^{-2}. Unless there is a more copious source of H^+ in the vicinity of 200 km altitude than our computations indicate, it is the internal kinetic pressure and possible magnetic fields that supply the necessary pressure.

DISCUSSION OF MODELS: $Q_{SW} = 0$

In support of this view, we obtained a series of temperature and density profiles for both the neutral and charged particle gases. The neutral helium density at 100 km and the effective magnetic dip angles were varied as parameters while all the remaining boundary conditions and solar EUV flux were held constant from model to model. From sets of profiles where the electron density $N_e \simeq 1.2 \times 10^4$, the charged particle pressure, $P_c = N_e\, kT_e + [H^+]\, kT_{H^+} + [D^+]\, kT_{D^+} + [He^+]\, kT_{He^+}$, at the upper boundary was obtained and is shown in Figure 4. The solid curves represent the kinetic pressure, P_c, and the dashed lines the difference between the solar wind pressure of the horizontal component, $B_t^2/8\pi$, of any magnetic field that may be present in the Venus ionosphere. At low helium densities the pressure decreases slowly with increasing amounts of helium forming a pressure minimum in the vicinity of $[He]_{100} = 5 \times 10^6\ cm^{-3}$. Further increases cause the pressure to rise very sharply. The reasons for this behavior are illustrated in Figure 5 where the temperature and pressure curves are given simultaneously. The topside density corresponding to each point on the pressure curve was $1.2 \times 10^4\ cm^{-3}$. It can be seen that the minimum in the pressure curve arises from decreasing ion temperatures as the ion thermal coupling to the neutral gas increases. Further increases in the neutral helium density cause the solar EUV heating of the electrons to increase at a much faster rate than the corresponding loss to the cooler ions and neutral gases. Therefore, at low neutral helium densities the pressure follows the ion temperature

while at higher densities it follows the electron temperature.

The solutions appropriate to Venus are where $P_c = P_{sw} - B_t^2/8\pi$. Clearly effective magnetic dip angles less than 4° are not possible since the resulting electron temperature and therefore P_c are too high for any concentration of neutral helium considered. Solutions for effective dip angles greater than 5° are not explicitly ruled out except that they require very high neutral helium concentrations or stronger magnetic fields than was measured on the nightside by Venera IV (Dolginov et. al., 1968). If Venus has only a weak intrinsic magnetic field (less than 10γ above 100 km altitude) that is essentially horizontal in the vicinity of the occultation point, or if there exists an externally generated field of similar nature, then the neutral helium concentration at 100 km is likely to be in the vicinity of 5×10^8 cm^{-3} (typical of the curve labelled dip = 4.1°). The total atmospheric content of He associated with this number density can be accumulated during 4.5×10^9 years, as long as the total escape rate of He is less than 10^6 cm^{-2} sec^{-1}. In the absence of any experimental evidence for an induced field, the Venera IV measurements of about 10γ form an upper limit to any intrinsic field. The case B = 0 is not allowed since a pressure balance cannot be achieved (it is equivalent to the Dip = 90° case). The dashed line labelled B = 0 should be interpreted as $0.01 \leq B \leq 0.05\gamma$, a field strength sufficient to reduce thermal conduction across field lines, yet small enough not to significantly affect the pressure balance (Leontovich, 1965).

As each point on the P_c curves in Figure 4 corresponds to a separate set of temperature and density profiles, we show a typical example of one of the allowed solutions, Figure 6, for a neutral helium density

of 5×10^{7} cm^{-3}, $P_c = 8.65 \times 10^{-9}$ dynes cm^{-2}, and solar EUV flux scaled from the values given by Hinterregger et. al., (1963). In this model the electron density has a peak of 5.2×10^{5} cm^{-3} at 140 km altitude in a region that is mainly CO_2^+. At 260 km the scale height rapidly increases as the ionic composition changes from CO_2^+ to the light ions He^+ and H^+. The profiles for H^+ and D^+ have been combined by summing. At 500 km, the ionopause is indicated schematically by the dashed line $P_c = P_w$. A very similar set of profiles is obtained when the quantity of neutral hydrogen and deuterium is increased so that He^+ becomes the minor ion. The only significant change is a further increase in scale height corresponding to the reduced average mass of the resulting ionosphere. These density profiles shown were computed self consistently with the temperatures shown in the other half of Figure 6. Here the temperatures just below the ionopause are T_n = 640 °K, T_e = 3670 °K T_{He^+} = 2160 °K, and T_{H^+} = 2330 °K. Because of the efficient transfer of thermal energy between the ions, T_{H^+} and T_{He^+} are closely coupled in the topside. In the lower region where the neutral helium density is much larger, the heat loss from He^+ to He predominates over the heat input from the electrons via the large momentum transfer cross section corresponding to the symmetric charge transfer reaction. Since the coupling of H^+ to the neutral atmosphere is not as efficient as He^+, T_{H^+} tends to follow T_e.

An interesting feature of the Venus thermal structure is the relative stability of the neutral gas temperature with respect to changes in neutral gas composition. An example of this is shown in Table 1 where

the CO_2 density is varied from $1x10^{12}$ cm^{-3} to $1x10^{14}$ cm^{-3} with little change in T_n. Unlike the similar case for the earth's ionosphere (Herman and Chandra, 1969) a single constituent, CO_2, is responsible for both the conversion of solar radiation into thermal energy and its subsequent reradiation in the infrared. Increasing the concentration of CO_2 for a given solar energy input redistributes both the energy absorption and reradiation to somewhat higher altitudes without altering the exospheric thermal balance.

SOLAR WIND HEATING: $Q_{sw} \neq 0$

The picture of the dayside ionosphere presented so far is one where a relatively static pressure balance is achieved as long as the solar wind streaming pressure remains constant. A decrease in the streaming pressure would require the ionopause boundary to move out a considerable distance from the planet to reestablish the necessary pressure balance. Since the solar wind streaming pressure is known to change quite frequently relative to the flux of solar radiation, the ionopause level would be constantly moving. This would mean the Mariner V data was transient in nature, and as such is merely a snapshot of a highly dynamic system. However, if the solar wind is responsible for about half of the charged particle heating within the ionosphere, for example by collisionless damping of fast mode hydromagnetic waves (Barnes, 1966) originating in the ionopause region, then reducing the solar wind streaming pressure leads to a corresponding reduction in ionospheric topside kinetic pressure. Using the expression $Q_{sw} = (\alpha V P_{sw}/\lambda) \exp((z-z_u)/\lambda)$ to simulate solar wind heating as a function of the parameters αV and λ, the resulting electron temperatures are shown in Figure 7 and the corresponding kinetic pressures in Table 2. When $\alpha V = 10^3$, the results are approximately the same as the case where there is no solar wind heating ($\alpha V=0$). For example, if the heating mechanism were to arise from waves propagating at approximately the acoustic speed of about 5×10^5 cm/sec, then the overall heating efficiency α would have to be 0.001 for the effect to be negligible. The overall heating efficiency is that fraction of the solar wind streaming energy that propagates downward from the ionopause and dissipates over distances of order of the

vertical extent of the ionosphere, $\lambda \sim 100$ km. As αV increases, the heating effect becomes very large, causing electron temperatures of 10^4 °K when $\alpha V = 10^6$. From Table 2, however, it can be seen that αV cannot exceed about 5×10^4 without the internal kinetic pressure exceeding the solar wind pressure. The values in Table 2 and the profiles in Figure 7 have been obtained for that density of neutral helium that produces a pressure minimum, see Figure 4, dip = 5°. When $\alpha V = 10^4$, Q_{sw} is approximately half the total heat input to the electrons in the topside of the ionosphere. If V is about the ion-acoustic speed and $\lambda \sim 10^7$ cm, then an efficiency of $\alpha = 1$ to 5% would lead to a nearly stable ionopause and topside ionosphere.

In the complete absence of a magnetic field in the topside ionosphere solar wind heating is insufficient to raise the electron and ion temperatures enough to maintain the ionopause. When the extreme upper limit for solar wind heating is used, $\alpha V = 10^5$ and $\lambda = 100$ km, the resulting charged particle pressure, P_c, is only 4×10^{-9} dynes cm^{-2}, a factor of two too small. With more likely values for Q_{sw}, $\alpha V \sim 10^4$ cm sec^{-1}, there must be an essentially horizontal magnetic field throughout a significant portion of the topside ionosphere. As mentioned earlier, moderate upward velocities will compress any horizontal components of a magnetic field into a restricted region below the ionopause. If the extent of this region, d_b, is about 100 km or larger, then sufficient heating occurs and a solution can be obtained. For a field of strength about 10γ and dip angle of 5°, $\alpha V = 10^4$ cm sec^{-1} and $\lambda = 100$ km, a suitable solution is found with neutral

helium densities at 100 km altitude in the vicinity of 10^{8} cm^{-3} for 100 km $\lesssim$ d_b $\lesssim$ 400 km.

At this time it is not possible to use the existing data to choose between the several models since each one leads to similar temperatures and densities for reasonable values of their parameters. The most likely choice should include a combination of all the effects we have discussed.

THE EFFECTS OF EDDY DIFFUSION

All of the models shown so far were computed for the case where the eddy diffusion coefficient was taken to be 10^6 cm^{-2} sec^{-1}. Eddy diffusion and thermal escape was incorporated into our computations of the neutral atmosphere in a manner similar to that of McElroy and Hunten (1969), as well as the additional effect of charged particle temperature coupling. An example of the dependence of eddy diffusion for neutral helium is given in Figure 8 for four values of K_{eddy}(0, $5x10^5$, $5x10^6$, and $5x10^7$ cm^2 sec^{-1}). The behavior of neutral helium is as expected; in the region dominated by CO_2, the scale height for neutral helium is approximately that of CO_2, while at higher altitudes the more usual scale height dominates. In the absence of eddy diffusion, $K_{eddy} = 0$, the reduced scale height effect persists since the effects of thermal diffusion are proportional to the strong temperature gradients in this region. Hydrogen because of its high bulk velocity does not show substantial dependence on either eddy or thermal diffusion. Even in the absence of eddy diffusion the neutral hydrogen is strongly depleted relative to a simple hydrostatic density distribution by the upward flux escaping the planet. Thus, if Venus has a relatively non-... bulent atmosphere between the cloud tops and 150 km, helium and deuterium are likely to be enhanced relative to hydrogen in both the neutral and ionic forms above 100 km altitude.

Since neutral helium and deuterium are strongly effected by eddy diffusion, the thermal structure of the ionosphere must also show corresponding effects, Figure 9. Above 200 km, increasing K_{eddy} decreases the amount of neutral helium and deuterium present so that the ion-neutral

thermal coupling is reduced and the ion temperatures rise. The effect on the electrons is quite different. Even though the heat loss to the ions and neutral gases is reduced, the heat input from the solar EUV is reduced even more to produce a net cooling effect. Since the electrons dominate the charged particle pressure, the upward pressure must also decrease. This means that the more turbulent the atmosphere, the more neutral helium will be needed to maintain the pressure balance under any fixed set of the other parameters.

Since the degree of turbulence in the lower ionosphere may be small relative to the similar height range on earth (McElroy and Hunten, 1969), a set of pressure curves is given for no eddy diffusion, Figure 10. As expected, the minimum in the P_c curves is shifted towards lower helium densities at 100 km (which become higher helium and deuterium densities above 250 km). In all other aspects the character of P_c for no eddy diffusion is very similar to the case where $K_{eddy} = 10^6$ cm^2 sec^{-1}. For a fixed set of parameters, $B_t = 10\gamma$, $\sigma W = 5 \times 10^3$, and a sufficient ionization rate to maintain the topside electron density, turbulence in the bottomside ionosphere shifts the likely neutral helium density at 100 km from 1×10^8 cm^{-3} to 5×10^8 cm^{-3}. Corresponding to one of the curves shown in Figure 10 (Dip = 4.1°), the topside thermal structure is shown in Table 3. Except for the shift in neutral helium density necessary to maintain about the same topside temperatures and densities, the essential features are unchanged. For the same topside pressure, P_c, the ion temperatures are slightly decreased and the electron temperature slightly increased in the absence of ionospheric turbulence. Therefore, while ultimately important

for quantitative agreement with more detailed data, eddy diffusion does not alter the qualitative results concerning the charged particles in the ionosphere even though the topside ion composition and thermal structure depend strongly on the degree of turbulence.

SUMMARY

Theoretical modeling of the daytime Venus ionosphere has been used in conjunction with the Mariner V data to help explain some of the observed features. The observed ionopause at 500 km altitude arises from the deflection of the incoming solar wind by the topside ionosphere. The resulting pressure balance between the solar wind and ionospheric kinetic and magnetic pressures leads to predictions of the thermal structure within the ionosphere. In order to achieve the required pressure balance a small essentially horizontal magnetic field must be present in the topside to reduce the effective thermal conductivity even when additional heating is supplied by the solar wind. Consistent with the thermal structure and the observation of about 10^4 electrons cm^{-3} in the topside ionosphere, the neutral helium density is likely to be in the range of $\sim 10^8$ cm^{-3} at 100 km. The actual value depends upon the degree of turbulence present in the lower ionosphere. With an eddy diffusion coefficient of 10^6 cm^2 sec^{-1} we find that the nearly isothermal topside electron and ion temperatures are approximately 4000 °K and 1300 °K respectively at the point corresponding to the Mariner V occultation data. The magnetic field for this case has a strength of about 10γ and a dip angle of 4.2°. Such a quantitative picture of the ionosphere is only tentative since most of the fundamental parameters, energy inputs and boundary conditions, are poorly known. In particular, a good quantitative picture would require a knowledge of ionospheric turbulence, the degree of solar wind heating, the densities of the light neutral constituents, H, D, and He, and the effect on the dayside ionosphere of lateral transport of H^+, D^+, and He^+ towards the nightside, which will have to be supplied by future measurements.

REFERENCES

1. Banks, P. Private Communication (1970)
2. Banks, P. and Axford, I., Nature, 225, 924 (1970)
3. Barnes, A., Phys. of Fluids, 9, 1483 (1966)
4. Barth, C.A., Wallace, L., and Pearce, J.B., J. Geophys. Res., 73, 2541 (1968)
5. Bauer, S., Hartle, R., and Herman, J., Nature, 225, 533 (1970)
6. Biondi, M.A., Annales De Géophysique, 20, 34 (1964)
7. Dalgarno, A. and Allison, A., J. Geophys. Res. 74, 4178 (1969)
8. Dessler, A.J., Atmospheres of Mars and Venus (edit. by Brandt, J.C., and McElroy, M.B.), 241 (Gordon and Breach, 1968)
9. Dolginov, S.S., Yeroshenko, E.G., and Zhuzgov, L.N., Kosmich. Issled., 6, 561 (1968)
10. Fjeldbo, G. and Eshleman, V.R., Radio Science, 4, 879 (1969)
11. Herman, J.R. and Chandra, S., Planet. and Space Sci., 17, 815 (1969)
12. Herman, J.R. and Chandra, S., Planet. and Space Sci., 17, 1247 (1969)
13. Hochstim, A.R., Kinetic Processes in Gases and Plasmas, Academic Press, N.Y. (1969)
14. Kurt, V.G., Dostovalow, S.B., and Sheffer, E.K., The Venus Atmosphere, (edit. by R. Jastrow and S.I. Rasool), 477, (Gordon and Breach, 1969).
15. Hinterregger, H., Hall, L., and Schmidtke, G., Space Research V, 1175 (1965)
16. Johnson, F.S., J. Atmos. Sci., 25, 658 (1968)

17. Leontovich, M.A., Reviews of Plasma Physics, Vol. 1, (Consultants Bureau, New York, 1964)

18. Knudsen, W.C., and Anderson, A.D., J. Geophys. Res., 74, 5629 (1969)

19. Mariner Stanford Group, Science, 158, 1678 (1967)

20. McElroy, M.B. and Hunten, D.M., J. Geophys. Res. 74, 1720 (1969)

21. McElroy, M.B., Astrophys. J., 150, 1125 (1967)

22. Paulson, J.F., Annales De Geophysique, 20, 75 (1964)

23. Spreiter, J.R., Summers, A.L., and Rizzi, A.W., Solar Wind Flow Past Non-Magnetic Planets - Venus and Mars, Dept. of Applied Mechanisms, Stanford University (1970).

ACKNOWLEDGEMENT

The authors gratefully acknowledge the extensive programming help and useful discussions of Mssrs. J. Bredekamp and P. Smidinger.

Figure Captions

1. Illustration of the solar wind encounter with Venus showing the bow shock and ionopause. The plane of the Venera and Mariner V orbits has been rotated into the plane normal to the Venus-Earth line.
2. A comparison of the effects of upward ionic bulk flow (solid lines) on the ionospheric thermal structure with a stationary ionosphere (dashed lines).
3. The electron density and ion composition when hydrogen (plus deuterium) is the dominant ion.
4. The pressure of the charged particles just below the ionopause level (500 km) at the Mariner V occultation point vs. the neutral helium density at 100 km altitude. The dashed lines represent the difference between the solar wind pressure and the magnetic pressure of the indicated field, $P_w - B_t^2/8\pi$. The cases shown are for magnetic dip angles between 1 and 10°, and $K_{eddy} = 10\ cm^2\ sec^{-1}$.
5. Topside electron and ion temperatures vs. the neutral helium density at 100 km altitude.
6. The ion composition and thermal structure when helium is the dominant ion in the topside. The parameters used are $\alpha V = cm\ sec^{-1}$, $\lambda = 100$ km, $K_{eddy} = 10^6\ cm^2\ sec^{-1}$, $[He]_{100\ km} = 5 \times 10^7\ cm^{-3}$, $[CO_2]_{100\ km} = 5 \times 10^{13}\ cm^{-3}$, $[He]_{100\ km} = 6 \times 10^6\ cm^{-3}$, $[D]_{100\ km} = 2 \times 10^6\ cm^{-3}$, and $[N_2]_{100\ km} = 10^8\ cm^{-3}$. The resulting topside charged particle pressure is 8.65×10^{-9} dynes cm^{-2}.

7. The effect of a nonthermal source of heating, Q_{sw}, originating in and above the ionopause region on the electron temperature. $Q_{sw} = (\alpha V P_w/\lambda)\exp((z-z_u)/\lambda)$. Solid lines represent λ = 300 km and the dashed lines λ = 100 km. I_n is the average of the neutral temperatures for all six cases shown with the spread indicated by the horizontal bars. $10^3 \leq \alpha V \leq 10^6$ cm sec^{-1} where α is the heating efficiency and V is the energy transport velocity.
8. The neutral helium density for values of the eddy diffusion coefficient ranging from 0 to $5x10^7$ cm^2 sec^{-1}. The dashed line represents the CO_2 density for comparison with the neutral helium scale height for the case where T_n = 650 °K.
9. The electron temperature for three values of the eddy diffusion coefficient. P_c is in units of 10^{-9} dynes cm^{-2} and the listed helium densities are calculated at 500 km altitude with a fixed value at the lower boundary (100 km), see Figure 8.
10. Charged particle pressure just below the ionopause vs. the neutral helium density at 100 km in the absence of eddy diffusion, K_{eddy} = 0. See Figure 4. The shaded region defines the range of allowed ionospheric solutions for the indicated magnetic field strengths.

APPENDIX I

The heat transport equations for the electrons, ions, and neutral gases are of the form

$$N_j k C_v \frac{\partial T_j}{\partial t} - \frac{\partial}{\partial z}\left[K_j(T_j)\frac{\partial T_j}{\partial z}\right] = Q_{js} + Q_{jp} - \sum_k L_{jk}\,(T_j - T_k)$$

N_j = density (cm^{-3}), k = Boltzmann's constant (ergs/^oK), C_v = specific heat (3/2 or 5/2), T_j = temperature of species j(^oK), K_j = thermal conductivity, Q_{js} = solar heat production (ergs cm^{-3} sec^{-1}), Q_{jp} = energetic particle heat production (ergs cm^{-3} sec^{-1}), L_{jk} = coefficient of the rate of energy exchange between gases, z - altitude (cm), t = time (sec).

For the electron gas:

$$K_e = 1.8 \times 10^{-5}\,\frac{T_e^{5/2}}{\ln\Lambda}$$

$$Q_{es} = \sum_j \sum_\lambda N_j\,\sigma_{j,\lambda}^{(I)}\,\epsilon_\lambda\,\phi_\lambda\,e^{-\tau_\lambda}$$

$$\tau_\lambda = \sum_s \frac{1}{\cos\chi}\int_\infty^z N_s(z')\,\sigma_{s,\lambda}^{(A)}\,dz'$$

$$Q_{ep} = \sum_i \frac{2\pi e^4\,n_e\,\ln\Lambda}{E_i}\left[\frac{m_i}{m_e}\,\mu_i(X_e) - \mu'_i(X_e)\right]\phi_i\,(E_i,z)$$

N_j = density of jth neutral species (cm^{-3}), $\sigma_{j,\lambda}^{(I)}$ = ionization cross section for wavelength λ (Hinteregger, et. al., 1965), $\sigma_{j,\lambda}^{(A)}$ = absorption cross section for wavelength λ (Hinteregger, et. al., 1965), ϵ_λ = heating efficiency at altitude z, ϕ_λ = solar EUV flux (cm^{-2} sec^{-1}) (Hinteregger, et. al., 1965), χ = solar zenith angle, $e = 4.803 \times 10^{-10}$ (e.s.u.), E_i = energy of incoming energetic ion (ergs), m_i = mass (gm).

$\phi\ (E_i,z)$ = flux of incoming energetic ions(cm^{-2} sec^{-1})

$$\mu_i\ (X_e) = \sqrt{\frac{2}{\pi}} \int_o^{X_e} \sqrt{t}\ e^{-t}\ dt = \text{erf}\ (X_e)$$

$$\mu_i'\ (X_e) = \sqrt{\frac{2}{\pi}}\ \sqrt{X_e}\ \ e^{-X_e}$$

$$X_e = \frac{m_e}{m_i}\ \frac{E_i}{kT_e}$$

Energy loss from electrons to neutrals

$$L_{en} = 1.602 \times 10^{-12}\ n_e(T_e - T_n)\{1.77 \times 10^{-19}$$

$$N_1\ (1\text{-}1.21 \times 10^{-4}\ T_e)\ T_e$$

$$+ 2.9 \times 10^{-14}\ N_1 T_e^{-1/2} + 3 \times 10^{-16}\ N_2\ (1\text{-}4.8 \times 10^{-5} T_e^{1/2})$$

$$+ 5.8 \times 10^{-14}\ N_2 T_e^{-1/2} + 1.8 \times 10^{-15}\ N_3(1 + 4.3 \times 10^{-4} T_e)$$

$$+ 1.72 \times 10^{-14} N_3 T_e^{-1/2} + 2.46 \times 10^{-17} N_4 T_e^{1/2}$$

$$+ 9.63 \times 10^{-16} N_5 (1-1.35 \times 10^{-4} T_e) T_e^{1/2}$$

$$+ 4.82 \times 10^{-16} N_6 (1-1.35 \times 10^{-4} T_e) T_e^{1/2}$$

$$+ 1.37 \times 10^{-14} N_2 \exp (2.72 \times 10^{-6} (T_e - T_n)^2$$

$$+ 6.43 \times 10^{-3} (T_e - T_n)\}$$

Energy loss from electrons to ions

$$L_{eI} = 5.18 \times 10^{-7} n_e n_I (T_e - T_I)/(A_I T_e^{3/2}) \ln\Lambda$$

$$A_1 = 28, A_2 = 44, A_3 = 2, A_4 = 4, A_5 = 1, A_6 = 2$$

corresponding to the ionic species N_2^+, CO_2^+, H_2^+, He^+, H^+, D^+, respectively.

$15 \leq \ln\Lambda \leq 20$ for the cases of interest

$$\sum_k L_{ek} (T_e - T_k) = L_{en} + \sum_I L_{eI}$$

Ion gases:

Only the light ions are assumed to have temperature significantly different from the neutral gas temperature T_n.

$$K_I = 7.37 \times 10^{-8} T_I^{5/2} A_I^{-1/2}$$

$$Q_{IS} = 0$$

$$Q_{IP} = 2\pi e^4 n_I \sum \frac{\phi_j (E_j)}{E_j} \ln\Lambda$$

Energy loss from He^+ to neutral gases

$$L_{4n} = n_4(T_4 - T_n)\left[1.21 \times 10^{-26} N_4 (T_4 + T_n)^{1/2} + 5.78 \times 10^{-26} N_1 + 6.47 \times 10^{-25} N_2 + 1.28 \times 10^{-25} N_3 + 1.09 \times 10^{-25} N_5 + 1.17 \times 10^{-25} N_6\right]$$

Energy loss from H^+ to neutral gases

$$L_{5n} = n_5(T_5 - T_n)\left[4.078 \times 10^{-26} N_5 (T_5 + T_n)^{1/2} + 2.59 \times 10^{-26} N_1 + 2.04 \times 10^{-26} N_2 + 1.41 \times 10^{-25} N_3 + 4.69 \times 10^{-26} N_4 + 1.28 \times 10^{-25} N_6\right]$$

$$S_{45} = 5.35 \times 10^{-16} \frac{n_4 n_5 (T_5 - T_4)}{A_4 A_5 \left[\frac{T_4}{A_4} + \frac{T_5}{A_5}\right]^{3/2}} = - S_{54}$$

= rate of heat exchange between ions 4 (He^+) and 5 (H^+)

$$\sum_k L_{jk} (T_j - T_k) = L_{jn} + S_{j,I} - L_{ej}$$

Deuterium, D^+, is assumed to have its temperature between T_4 and T_5. This causes little error since T_4 is close to T_5 at all altitudes.

Neutral Gases:

All the neutral gases are assumed to have a common temperature T_n.

$$K_n = \frac{\sum_{s=1}^{6} F_s N_s}{\sum_{s=1}^{6} N_s} T_n^{1/2}$$

$F_1 = 236$ $F_2 = 209$ $F_3 = 1880$ $F_4 = 875$ $F_5 = 2080$ $F_6 = 1470$

$$Q_{ns} = \sum_{\lambda} \sum_{s=1}^{6} \epsilon_{n\lambda} \sigma_{s\lambda}^{(A)} I_\lambda N_s e^{-\tau_\lambda}$$

$$I_\lambda = \frac{hc}{\lambda} \phi_\lambda$$

$$Q_{np} \simeq 0$$

Radiative Enery Loss from Neutral Gas

$$L_{nr} = 2.52 \times 10^{-22} N_2 \sum_{s=1}^{6} N_s \exp\left[-\frac{960}{T_n} - 82.8\ T_n\right]^{-1/3}$$ (McElroy, 1967)

$$N_s(z) = \frac{N_s(z_L)\ T_n(z_L)}{T_n(z)} \exp\left\{ - \int_{z_L}^{z} \frac{dz'}{H_s} - \int_{z_L}^{z} \frac{K(\frac{1}{H_a} - \frac{1}{H_s}) + \frac{D_s \alpha_s}{T_n} \frac{\partial T_n}{\partial z} + V_{sB}}{D_s + K} dz' \right\}$$

$$H_s = \frac{kT_n}{m_s g} \qquad H_a = \frac{kT_n}{m_a g} \qquad m_a = \frac{\sum_{s=1}^{6} m_s N_s}{\sum_{s=1}^{6} N_s}$$

$K = K_{eddy}$, the coefficient of eddy diffusion

$$D_s = \left[\sum_j \frac{N_j}{b_{sj}}\right]^{-1} \quad \text{(McElroy and Hunten, 1969)}$$

$$b_{sj} = \frac{3}{8\sigma_{ij}^2}\left[\frac{k\ T_n(m_s + m_j)}{2\pi\ m_s\ m_j}\right]$$

$\alpha_s = -1/4$ = thermal diffusion coefficient (McElroy and Hunten, 1969)

$$\sigma_{ij} = 1/2\ (\sigma_i + \sigma_j)$$

$$\sigma_i = 3.68 \times 10^{-8} \qquad \sigma_2 = 4.0 \times 10^{-8} \qquad \sigma_3 = 2 \times 10^{-8}$$

$$\sigma_4 = 3 \times 10^{-8} \qquad \sigma_5 = 1.06 \times 10^{-8} \qquad \sigma_6 = 1.06 \times 10^{-8}$$

$$V_{sb}\ (z) = N_s\ (z_{esc})\ V_{sb}\ (z_{esc})/N_s\ (z)$$

$V_{sb}\ (z_{esc})$ = Jeans escape velocity for species s.

$$g\ (z) = 877\left[\frac{6.056 \times 10^8}{6.056 \times 10^8 + z}\right]^2$$

$$\sum_k L_{nk}\ (T_n - T_k) = L_{nr} - \sum_I L_{In} - L_{en}$$

The momentum and continuity equations have the general form

$$m_i n_i \frac{\partial V_i}{\partial t} + V_i \frac{\partial V_i}{\partial z} = -\frac{\partial p_i}{\partial z} - m_i n_i g + e_i n_i E - \sum_j K_{ij}\ (V_i - V_j)$$

$$\frac{\partial n_i}{\partial t} + \frac{\partial}{\partial z}\ (V_i n_i) = P_i - L_{pi}$$

Because of the presence of the Venus plasmapause at an altitude of 500 km acting as a cap on the ionosphere, the vertical flow velocities are likely to be small. Specifically, for $|V_i - V_j| < 10^4$ cm/sec the Venus ionosphere can be well represented by the static equations ($V_i \simeq 0$) for the light ions.

$$-\frac{\partial p_i}{\partial z} - m_i n_i g + e_i n_i E = 0$$

and

$$n_e = \sum_i n_i \quad \text{(charge neutrality)}$$

$$p_i = n_i k T_i$$

The heavier ions, CO_2^+ and N_2^+ are assumed to be in photochemical equilibrium throughout their region of importance.

$$N_2^+ + CO_2 \xrightarrow{k_1} N_2 + CO_2^+ \qquad k_1 = 9 \times 10^{-10}$$

$$CO_2^+ + e \xrightarrow{k_2} CO + O \qquad k_2 = 3.8 \times 10^{-7}$$

$$N_2^+ + e \xrightarrow{k_3} N + N \qquad k_3 = 2.9 \times 10^{-7}$$

$$\left.\begin{aligned} h\nu + CO_2 &\rightarrow CO_2^+ + e \\ h\nu + N_2 &\rightarrow N_2^+ + e \end{aligned}\right\} \quad \text{Hinteregger et. al (1963)}$$

Reactions with the light species:

The following table summarizes the charge transfer cross sections and electron recombination cross sections used in this work.

$$A + B^+ \rightarrow A^+ + B + \Delta E$$

Ionization Potential	Species		Energy Def.	Reac. Rate		Polariza-bility
IP ev	A	B^+	ΔE ev	k cm^{-3} sec^{-1}	(Ref)	α cm^3
13.595	H	H^+	0	3.49(-9)	Calc**	6.70(-25)
	H	He^+	10.991	2.76(-9)	"	
	H	CO_2^+	0.193	2.50(-9)	"	
	H	N_2^+	1.981	2.51(-9)	"	
24.586	He	H^+	-10.991	0		2.10(-25)
	He	He^+	0			
	He	CO_2^+	-10.798	0		
	He	N_2^+	- 9.010	0		
13.788	CO_2	H^+	- 0.193	5.6(-11)	Calc*	2.59(-24)
	CO_2	He^+	10.798	1.2(-9)	Paulson, 1963	
	CO_2	CO_2^+	0	1.3(-9)	Banks, 1970	
	CO_2	N_2^+	1.788	1.17(-9)	Calc**	
15.576	N_2	H^+	- 1.981	0		1.76(-24)
	N_2	He^+	9.010	1.5(-9)	Paulson, 1963	
	N_2	CO_2^+	-1.788	0		
	N_2	N_2^+	0			
	e	H^+	13.595	5.(-12)	Biondi, 1963	-----
	e	He^+	24.586	5.(-12)	"	
	e	CO^+	13.788	3.8(-7)	McElroy 1969	
	e	N_2^+	15.576	2.8(-7)	Biondi 1963	

* (Hochstim, 1969)

Table 1

PARAMETRIC VARIATION OF
NEUTRAL CARBON DIOXIDE

CO_2	T_e	T_{He^+}	T_{H^+}	T_n	Ne_p	Z_p
$1x10^{12}$	4470	1380	1450	644	$5.21x10^5$	120
$5x10^{12}$	4380	1420	1490	644	$5.23x10^5$	130
$1x10^{13}$	4300	1440	1510	643	$5.21x10^5$	130
$5x10^{13}$	4350	1750	1550	634	$5.33x10^5$	140
$1x10^{14}$	4300	1510	1580	645	$5.51x10^5$	145

α_W / λ	10^3	10^4	10^5	10^6
100 km	4.88×10^{-9}	5.77×10^{-9}	1.10×10^{-9}	2.80×10^{-8}
300 km	4.83×10^{-9}	5.21×10^{-9}	8.51×10^{-8}	2.15×10^{-8}

Table 2

The Effect of Solar Wind Heating on Charged Particle Pressure P_c

N_{He}	T_e	T_{He^+}	T_{H^+}	T_n
$5x10^4$	3810	3310	3360	683
$5x10^5$	3800	3250	3310	683
$5x10^6$	3750	2840	2960	682
$5x10^7$	3870	1700	1890	680
$5x10^8$	5780	856	955	658
$5x10^9$	10,600	643	690	625

Table 3

Topside Temperatures vs Neutral Helium Density
at 100 km. $K_{eddy} = 0$. Dip = 4.1

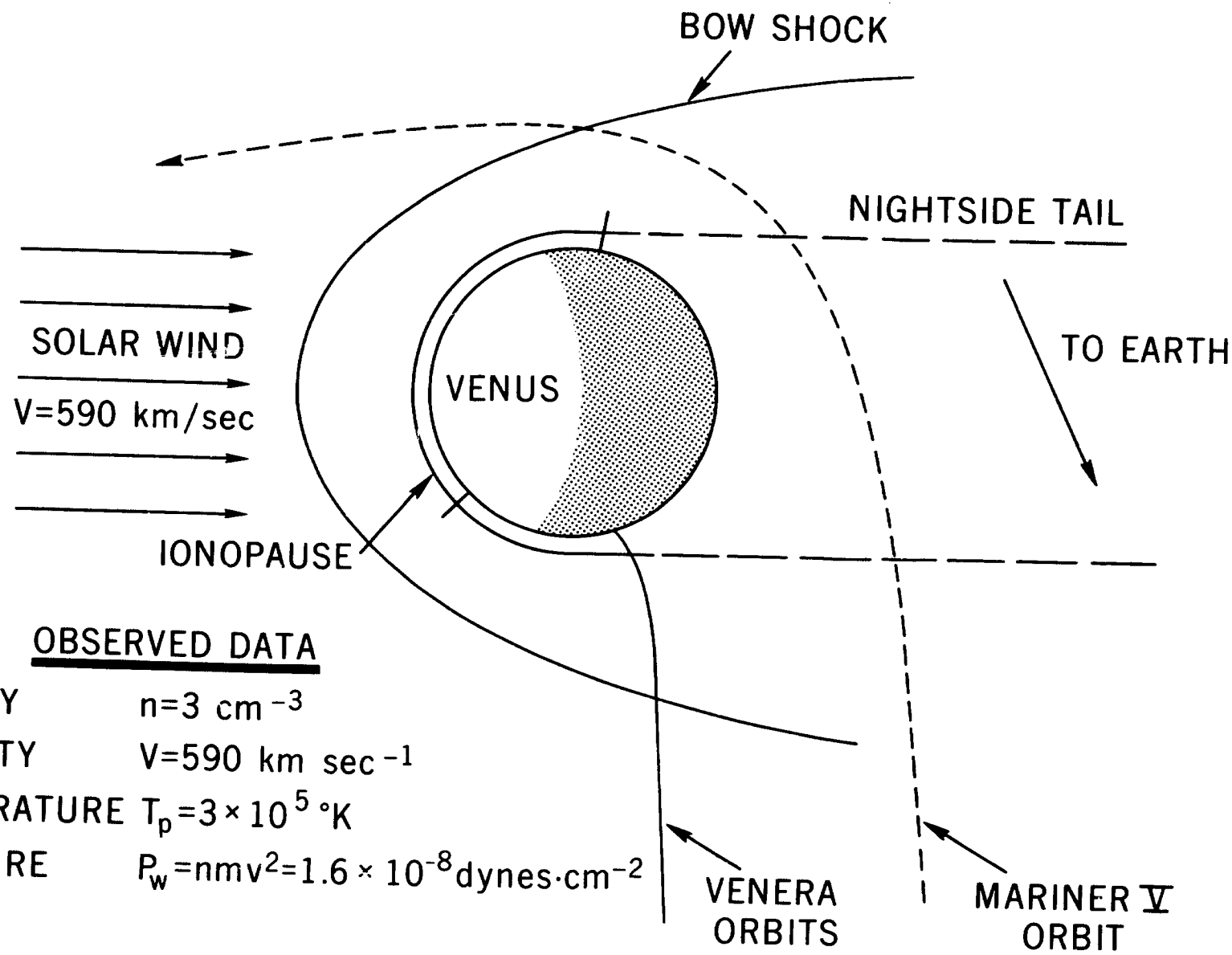

OBSERVED DATA

DENSITY	$n=3\ cm^{-3}$
VELOCITY	$V=590\ km\ sec^{-1}$
TEMPERATURE	$T_p=3\times10^5\ °K$
PRESSURE	$P_w=nmv^2=1.6\times10^{-8} dynes\cdot cm^{-2}$

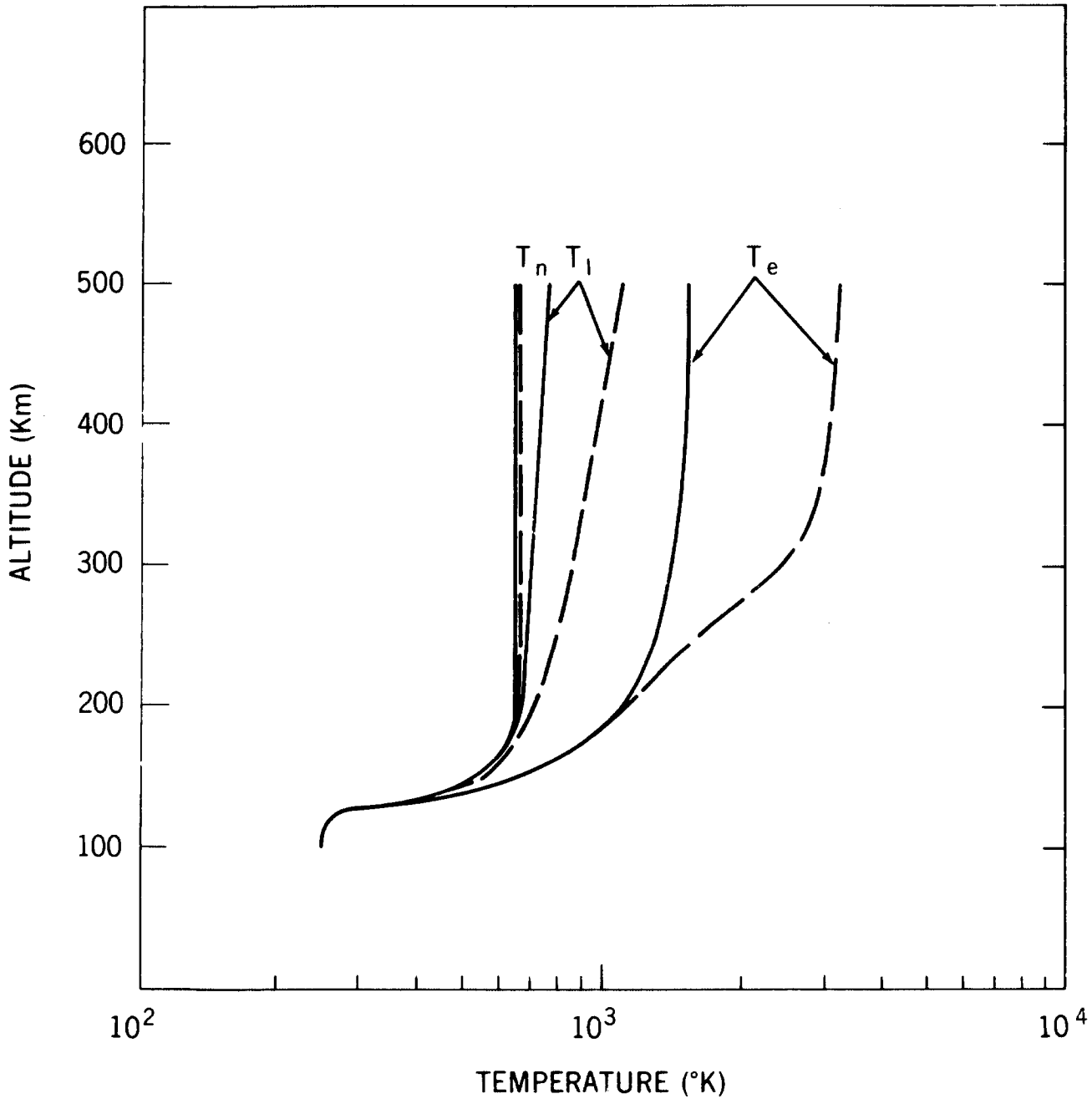
600
500
400
300
200
100
ALTITUDE (Km)
T_n
T_i
T_e
10^2
10^3
10^4
TEMPERATURE (°K)

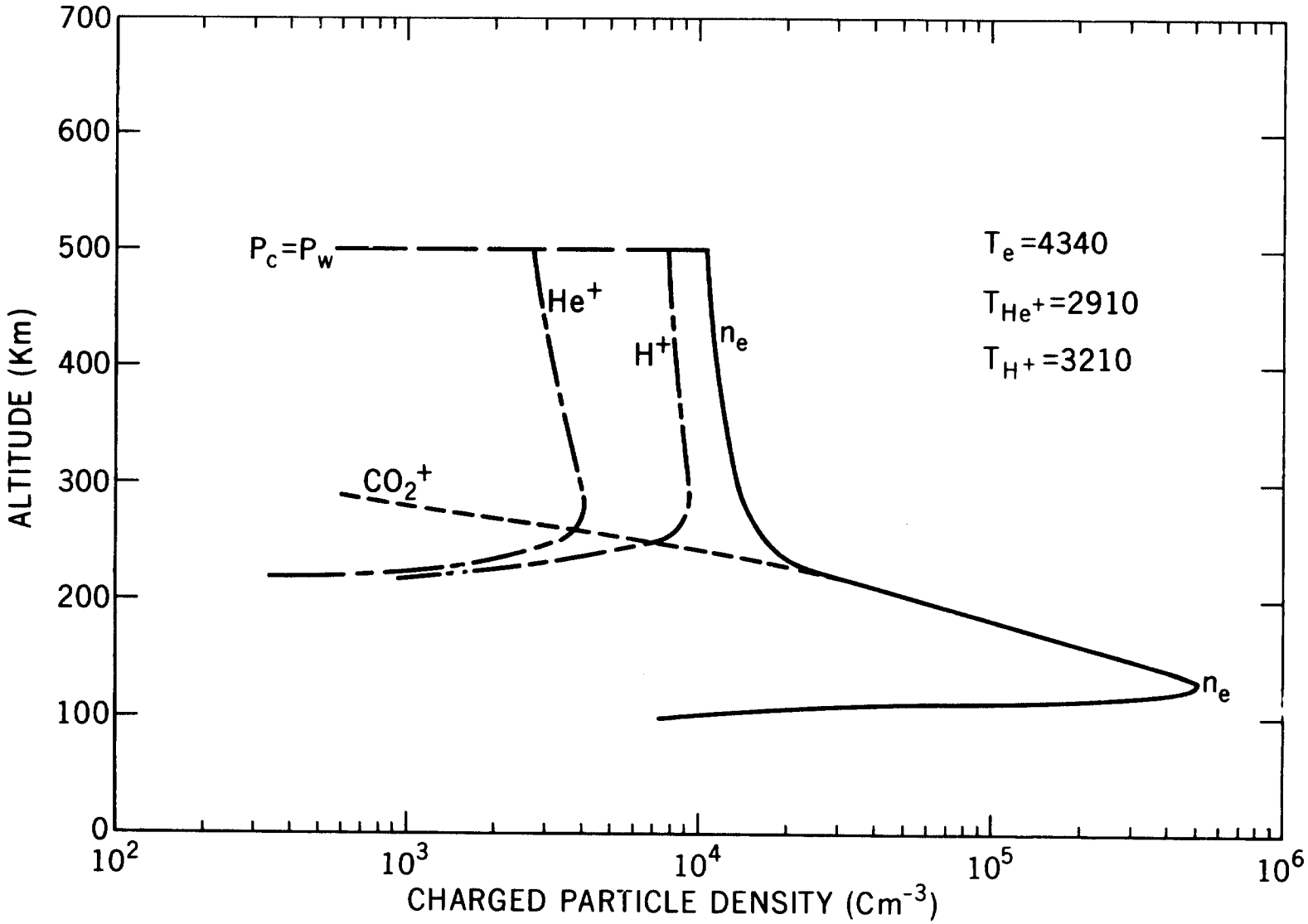
700
600
500
400
300
200
100
0
ALTITUDE (Km)
$P_c=P_w$
He^+
H^+
n_e
CO_2^+
n_e
$T_e=4340$
$T_{He^+}=2910$
$T_{H^+}=3210$
10^2
10^3
10^4
10^5
10^6
CHARGED PARTICLE DENSITY (Cm^{-3})

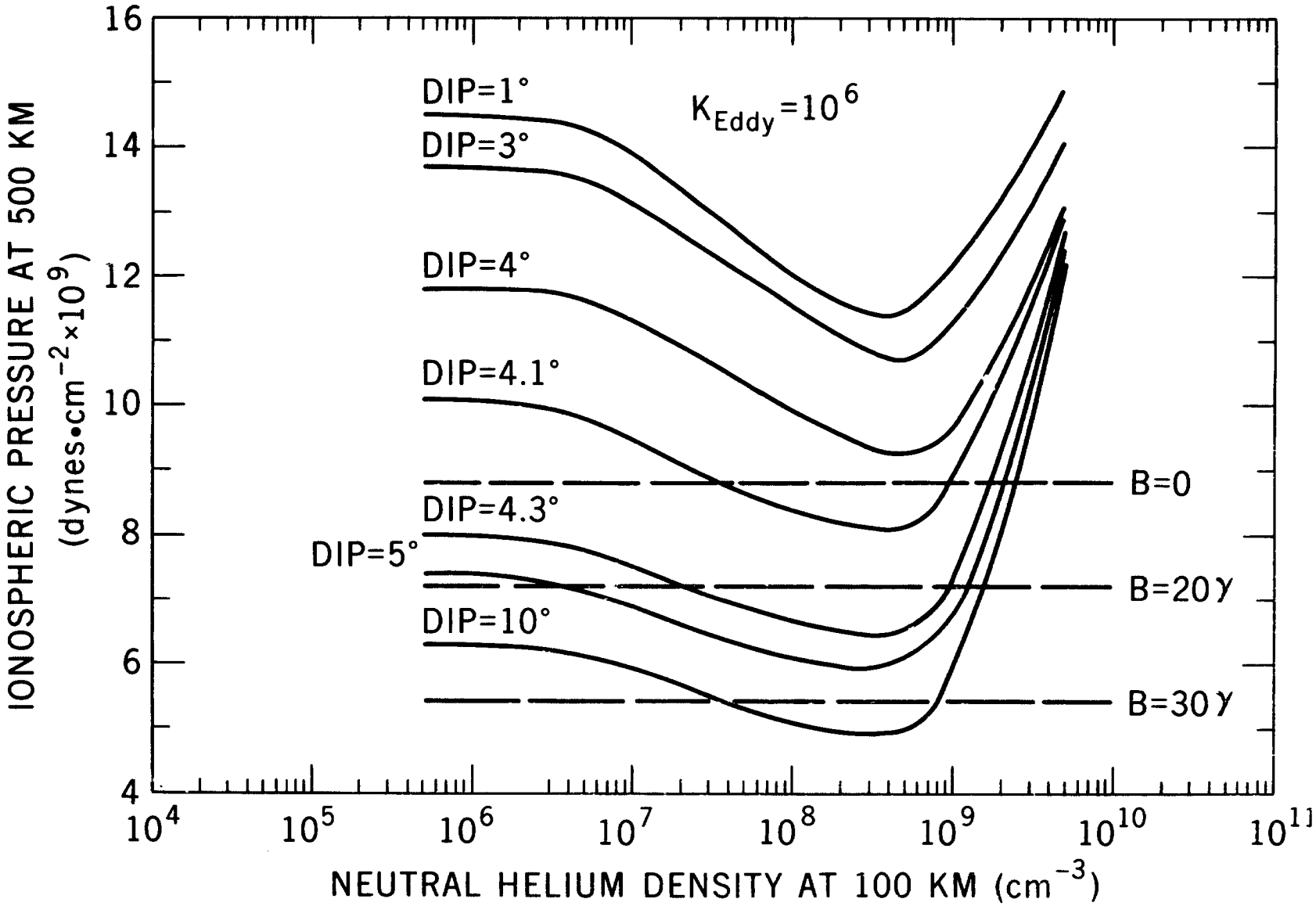
IONOSPHERIC PRESSURE AT 500 KM
(dynes•cm^{-2}×10^{9})
16
14
12
10
8
6
4
DIP=1°
DIP=3°
$K_{Eddy}=10^{6}$
DIP=4°
DIP=4.1°
B=0
DIP=4.3°
DIP=5°
B=20γ
DIP=10°
B=30γ
10^{4}
10^{5}
10^{6}
10^{7}
10^{8}
10^{9}
10^{10}
10^{11}
NEUTRAL HELIUM DENSITY AT 100 KM (cm^{-3})

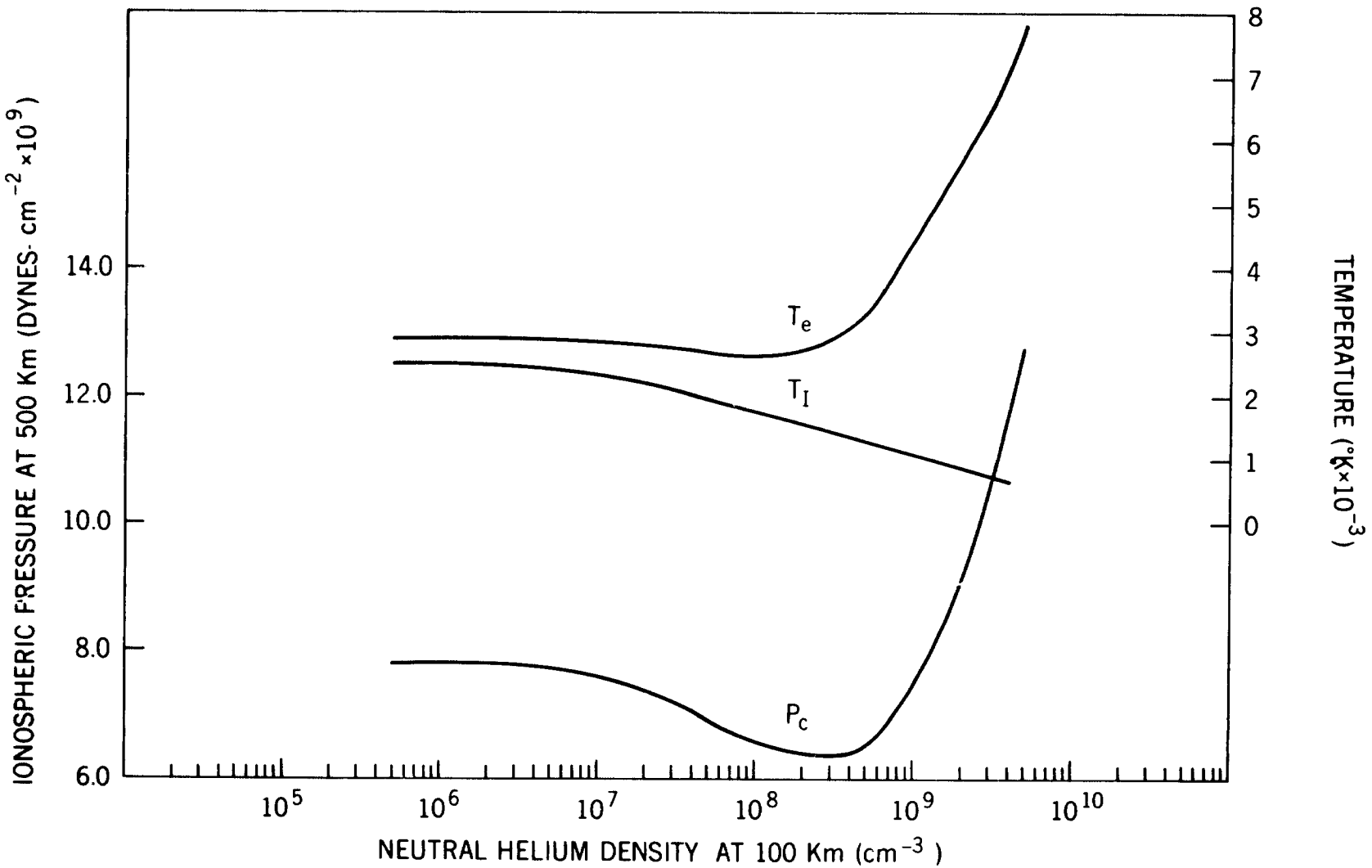
IONOSPHERIC PRESSURE AT 500 Km (DYNES· cm^{-2} ×10^{9})
14.0
12.0
10.0
8.0
6.0
T_e
T_I
P_c
8
7
6
5
4
3
2
1
0
TEMPERATURE (°K×10^{-3})
10^5
10^6
10^7
10^8
10^9
10^{10}
NEUTRAL HELIUM DENSITY AT 100 Km (cm^{-3})

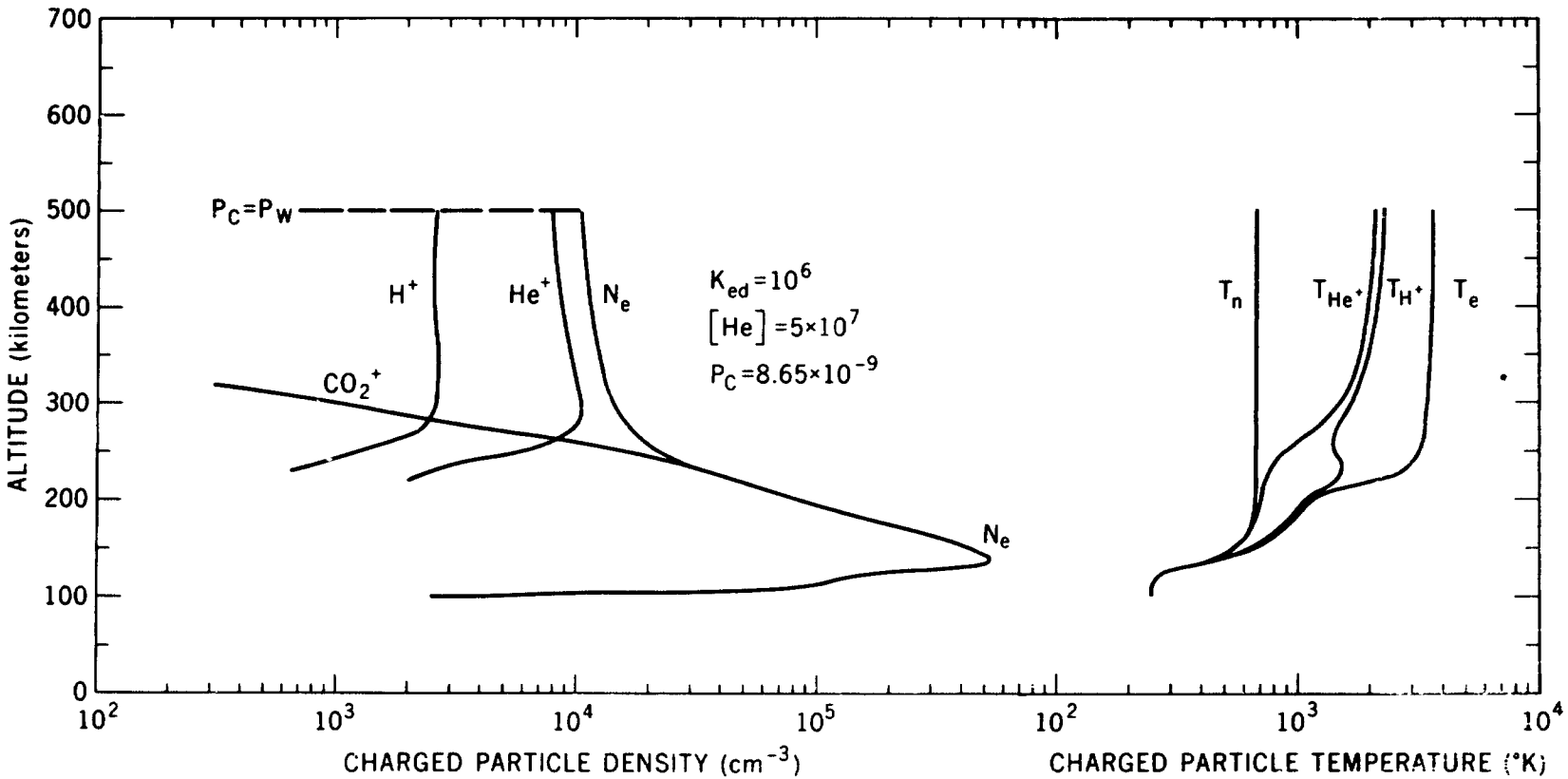
700
600
500
400
300
200
100
0
ALTITUDE (kilometers)
$P_C=P_W$
H^+
He^+
N_e
CO_2^+
$K_{ed}=10^6$
$[He]=5\times10^7$
$P_C=8.65\times10^{-9}$
N_e
T_n
T_{He^+}
T_{H^+}
T_e
10^2
10^3
10^4
10^5
10^2
10^3
10^4
CHARGED PARTICLE DENSITY (cm^{-3})
CHARGED PARTICLE TEMPERATURE (°K)

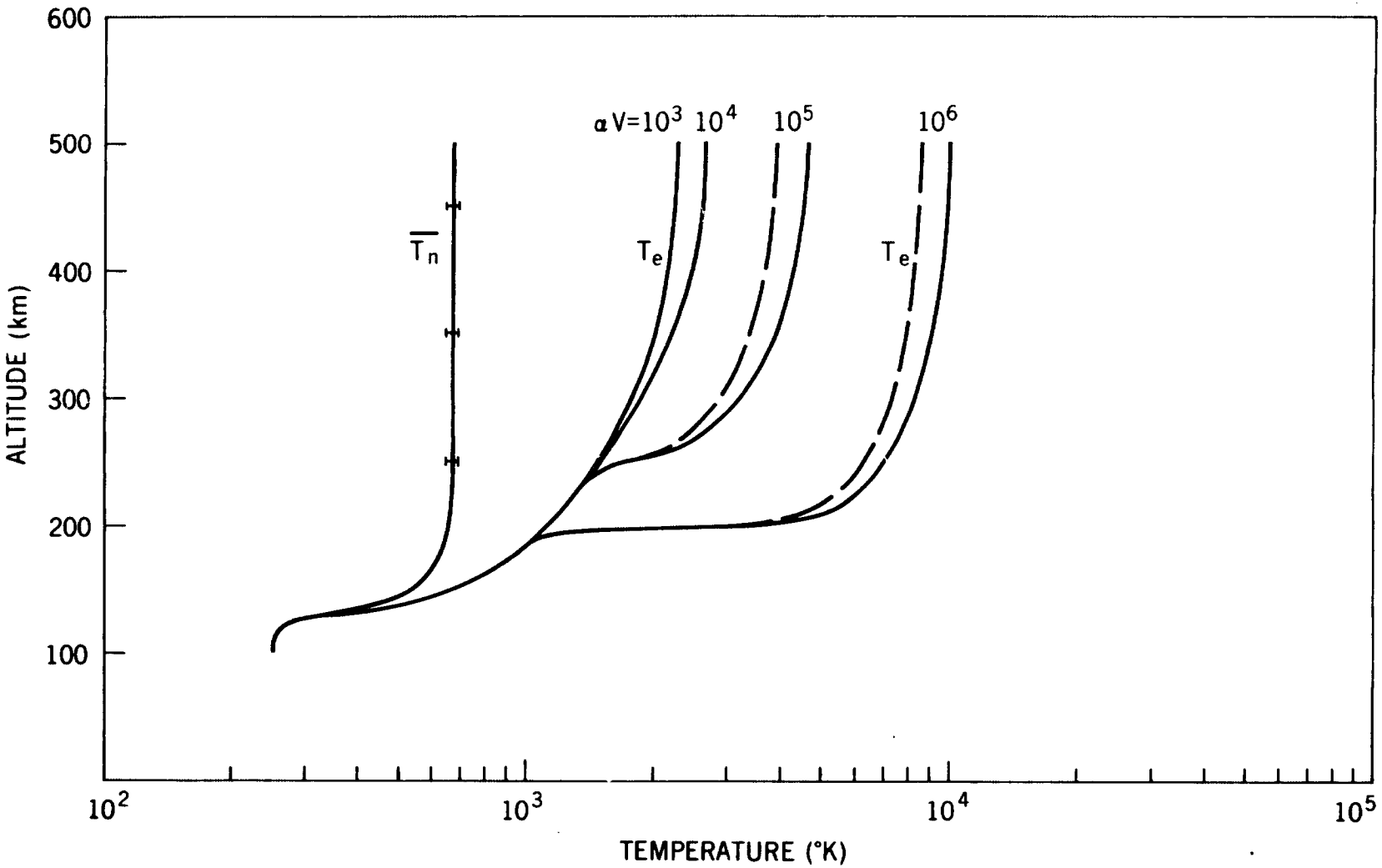
600
500
400
300
200
100
ALTITUDE (km)
$\alpha V=10^3$ 10^4 10^5 10^6
$\overline{T_n}$
T_e
T_e
10^2
10^3
10^4
10^5
TEMPERATURE (°K)

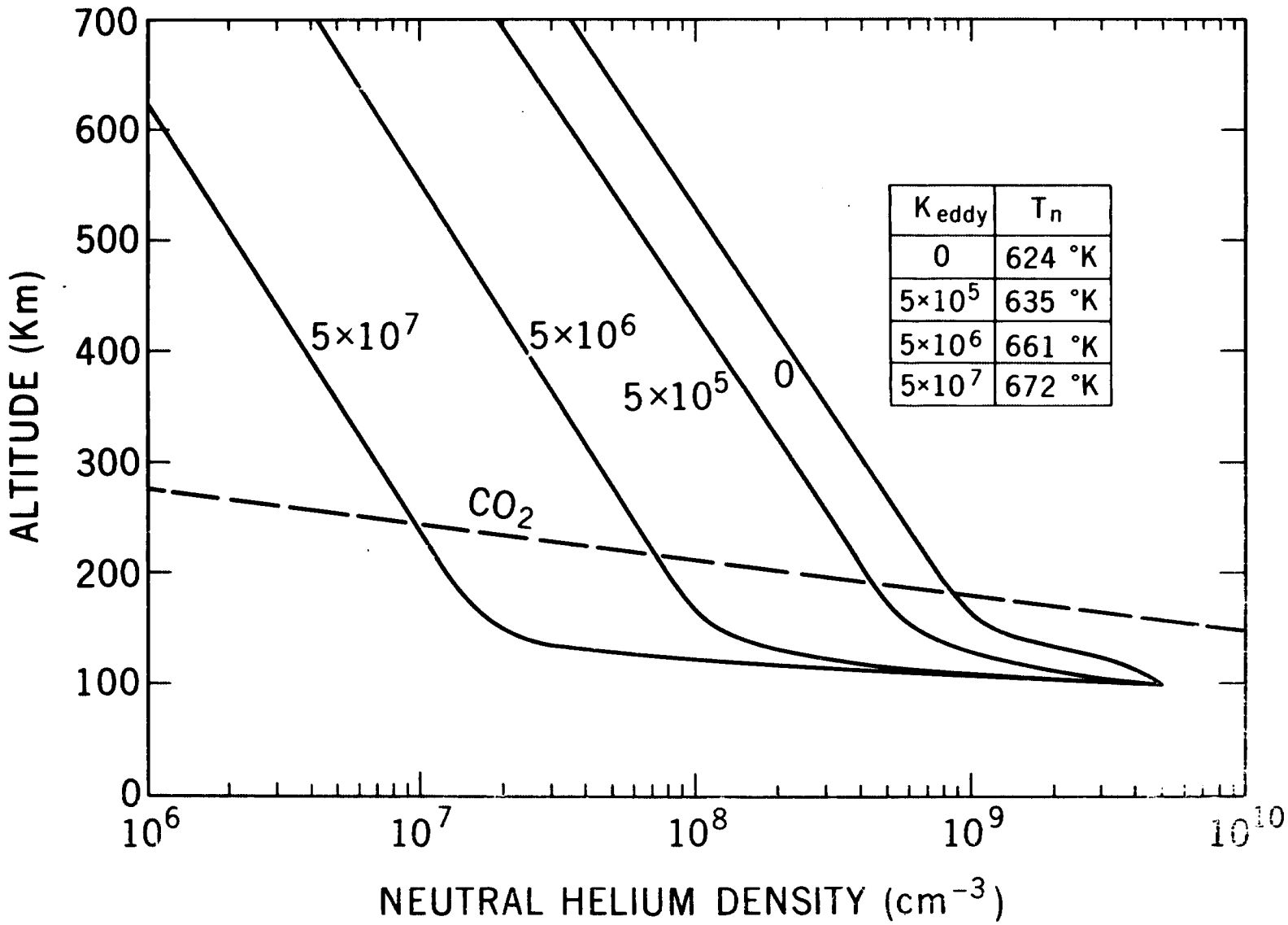
700
600
500
400
300
200
100
0
ALTITUDE (Km)
5×10^7
5×10^6
5×10^5
0
CO_2
10^6
10^7
10^8
10^9
10^{10}
NEUTRAL HELIUM DENSITY (cm^{-3})
K_{eddy} | T_n
0 | 624 °K
5×10^5 | 635 °K
5×10^6 | 661 °K
5×10^7 | 672 °K

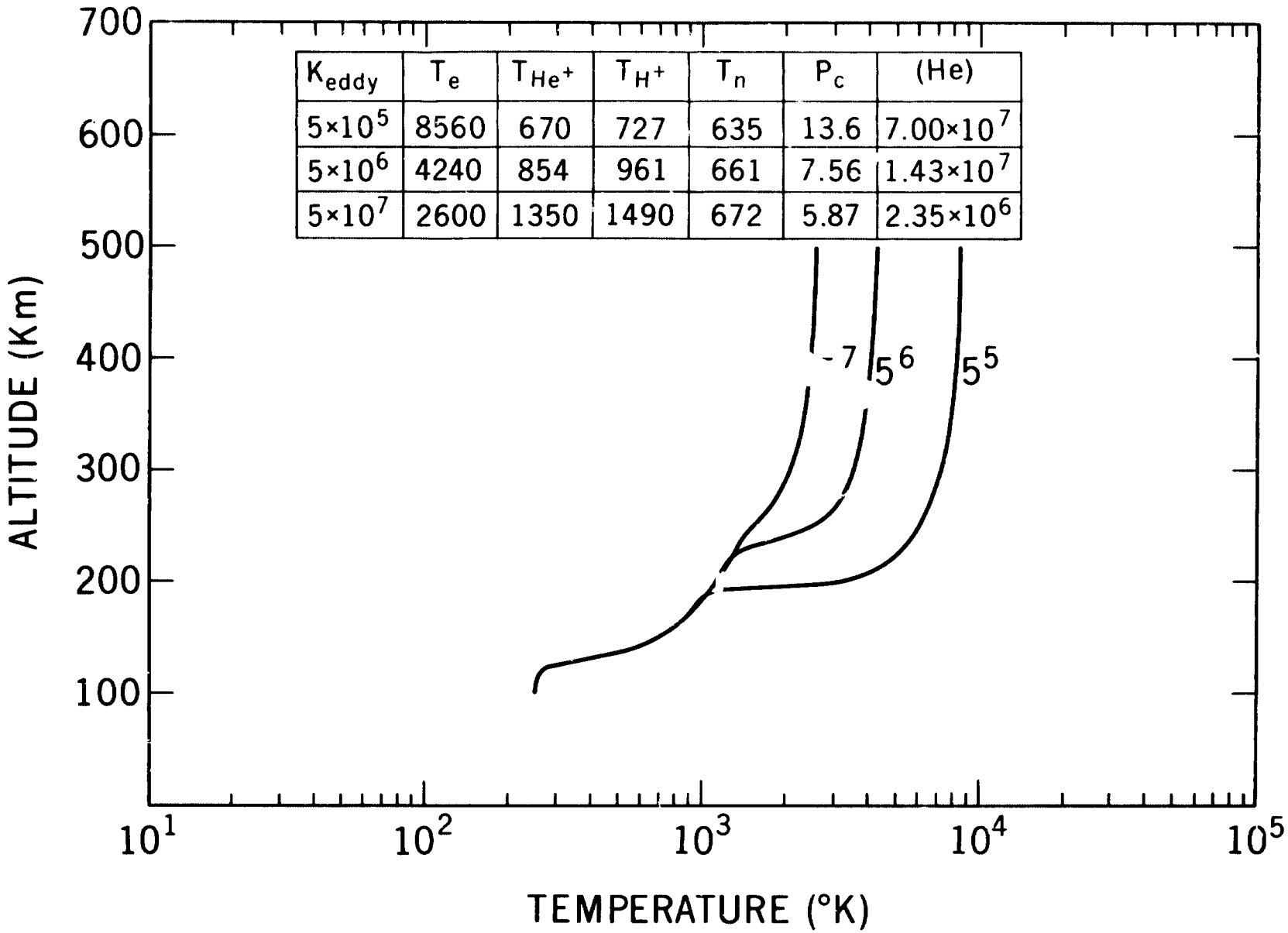

K_{eddy}	T_e	T_{He^+}	T_{H^+}	T_n	P_c	(He)
5×10^5	8560	670	727	635	13.6	7.00×10^7
5×10^6	4240	854	961	661	7.56	1.43×10^7
5×10^7	2600	1350	1490	672	5.87	2.35×10^6

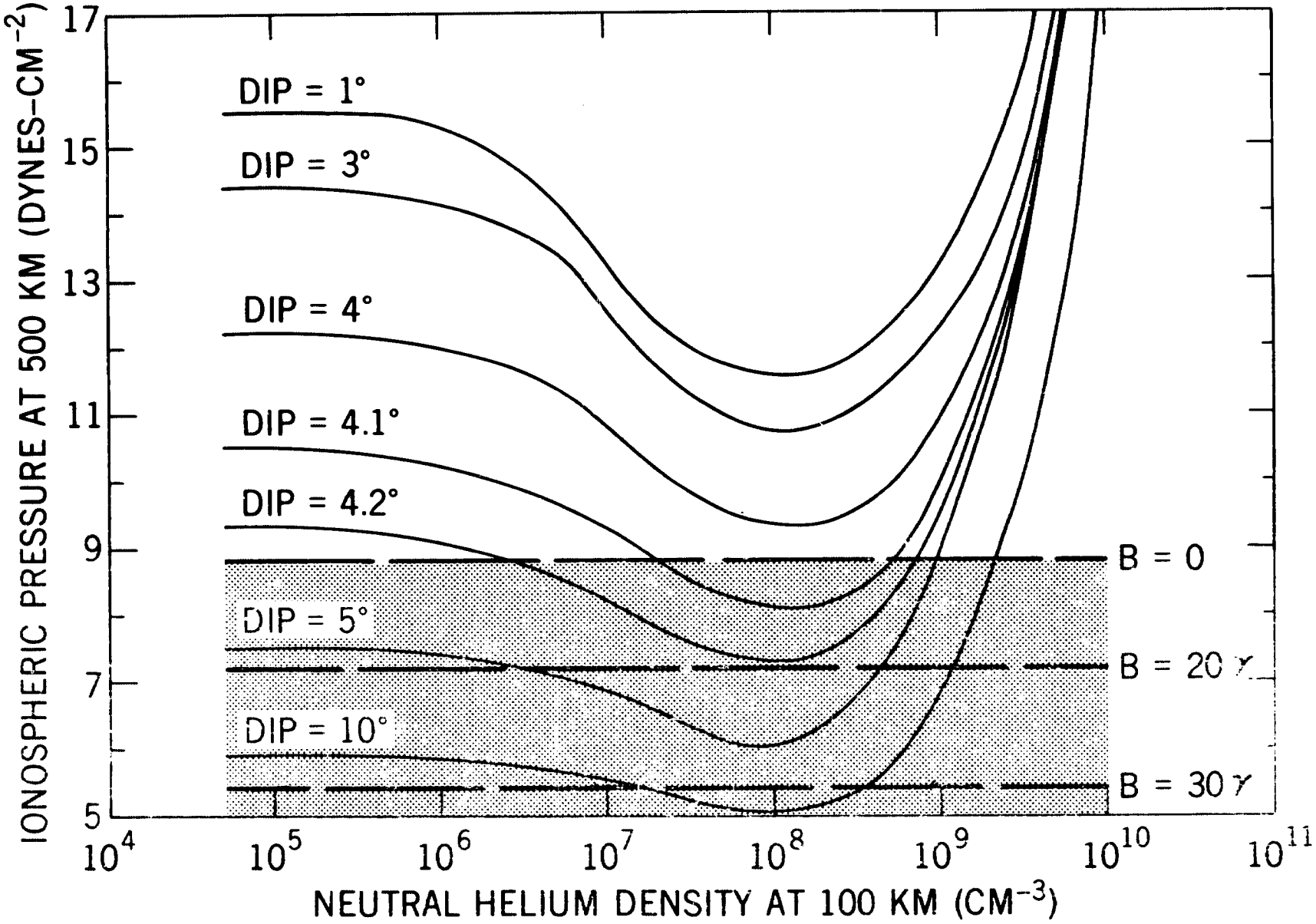
IONOSPHERIC PRESSURE AT 500 KM (DYNES-CM^{-2})
17
15
13
11
9
7
5
DIP = 1°
DIP = 3°
DIP = 4°
DIP = 4.1°
DIP = 4.2°
DIP = 5°
DIP = 10°
B = 0
B = 20 γ
B = 30 γ
10^4
10^5
10^6
10^7
10^8
10^9
10^{10}
10^{11}
NEUTRAL HELIUM DENSITY AT 100 KM (CM^{-3})